Superalloys 2012: 12th International Symposium on Superalloys
Edited by: Eric S. Huron, Roger C. Reed, Mark C. Hardy, Michael J. Mills, Rick E. Montero, Pedro D. Portella, Jack Telesman
TMS (The Minerals, Metals & Materials Society), 2012

RELATIVE CONTRIBUTIONS OF SECONDARY AND TERTIARY γ' PRECIPITATES TO INTERGRANULAR CRACK GROWTH RESISTANCE IN IN100 ALLOY

Kimberly Maciejewski[1], Hamouda Ghonem[1]
[1]Department of Mechanical Engineering, University of Rhode Island, Kingston, RI 02881, USA

Keywords: Nickel-based superalloy, Crack Growth, Precipitates, Grain Boundary, Heat Treatment, Yield Strength

Abstract

This paper examines the role of secondary and tertiary γ' on intergranular crack growth rate in P/M IN100. A series of different heat treatments were carried out on the as received material to vary the γ' statistics (size and volume fraction) through control of the different features of the heat treatment cycle. Dwell fatigue crack growth experiments have been performed on as received as well as heat treated specimens at 650°C and 700°C in air with dwell time loading cycles. Results on the as-received material show that the intergranular crack growth rate while temperature dependent, is independent of the hold time period. For the modified microstructures tested at 650°C, the dwell crack growth rate is shown to be sensitive to γ' variations. Considering that the yield strength of the continuum is a function of γ' statistics, the role of γ' on intergranular cracking was illustrated by correlating the crack growth rate and the continuum yield strength. This inverse relationship is examined numerically by modelling the grain boundary fracture path as an interface surrounded by near and far field continuum regions represented by viscoplastic flow formulations. Results of the model show that an increase in the continuum yield strength is accompanied by a lower viscous strain, resulting in higher constraint on the grain boundary sliding and thus, a decrease in the crack growth rate. This observation was further examined by calculating the individual components of yield strength associated with tertiary and secondary γ' precipitates. These components were correlated with the crack growth rate, showing higher sensitivity to the tertiary γ' precipitate hardening effects.

Introduction

A considerable amount of research has been performed on the crack growth damage mechanisms in precipitation strengthened nickel based superalloys. A segment of these studies has focused on the crack growth correlations with grain boundary (GB) phases and γ' precipitates within the γ matrix [1-3]. These precipitates are quantified in terms of primary (γ'_p), secondary (γ'_s) and tertiary (γ'_t) gamma prime. The work of Pang and Reed [4] have shown that large grain size, large coherent γ'_p size and higher volume fractions of both γ'_s and γ'_p precipitates improve fatigue lifetimes in P/M Ni-base alloys. Other studies have shown that the increase in the sizes of γ'_s and γ'_t are beneficial to fatigue crack growth. The work of Telesman et al [5] found that a larger γ'_s precipitate size, increases the resistance to hold time crack growth. Schirra et al [6] have shown that the γ'_s and γ'_t precipitates had small effects on mechanical properties of two P/M superalloy materials, KM4 and SR3, at 649°C. The strength of both alloys decreased with larger grain sizes and larger γ'_s sizes. While there was no effect of γ'_t size on strength, increasing γ'_t size had beneficial effects on increasing the crack growth resistance. Merrick and Floreen [7] have also observed that large size, uniformly distributed γ', as well as increased grain sizes, would decrease the intergranular crack growth rate. Knowles and Hunt [8] found that crack tip relaxation is induced by dissolution of fine γ'_t precipitates and selective coarsening of gamma prime decreases crack growth rate. Ma et al [9] in their work on IN783, did not observe a reduced intergranular crack growth rate due to the dissolution of particles, but due to the increase of the secondary γ' size. Recent work by Telesman et al [10] has shown that there is no influence of the GB $M_{23}C_6$ phase on hold time crack growth rate and that the key influence arises from the size of γ'_t. The authors suggest that the γ'_t plays an important role in reducing the crack tip driving force by crack tip relaxation, especially during long hold times. Their work, on LSHR alloy at 704°C, showed that an increase in γ'_t size is associated with a lower remaining stress level (more stress relaxation) and lower crack growth rate. This work has dealt with a superalloy having 5-10% of γ'_s and γ'_t, in the range of 50-55%. Similarly, Schirra et al [6], Gayda and Miner [11] have shown that increasing γ'_t size had beneficial effects on increasing the crack growth resistance. On the other hand, Jackson [12] considers that in nickel based superalloys neither the size nor the volume fraction of the γ' precipitates influence intergranular cracking unless they are in the direct vicinity of the carbides along the grain boundaries.

The studies mentioned above point out to different views of the role of microstructure in the intergranular cracking process. The primary objective of this study is to examine the influence of precipitates on the intergranular crack growth in IN100 alloy. This influence is assumed to exist based on the view that intergranular crack growth, which occurs as the decohesion of the GB interface in the crack tip region, is governed by the GB traction-displacement relationships in both normal and shear directions. These displacements are related, through compatibility requirements, to the deformation field in the immediate continuum surrounding the affected GB path. Localization of GB stress and strain would then depend on the corresponding fields in the immediate neighboring continuum. From this point of view, it is important to examine the role of microstructure in relation to the intergranular crack growth process. In sub-solvus heat treated IN100, the basic microstructural elements, in addition to grain boundaries and GB precipitates, are the primary, secondary and tertiary precipitates. The γ'_p are located throughout the matrix, particularly at triple points along grain boundaries and have long-time stability. These particles have been reported to have the same nanohardness as the gamma matrix [13], so they are considered to effectively contribute to the deformation process similar to the γ matrix and do not contribute additional hardening effects. On the other hand, the γ'_s and γ'_t are intragranular particles distributed within the γ matrix and act as barriers to dislocation motion and as such, contribute to the hardening processes. This paper focuses on effects of size and volume fraction of γ' on dwell crack growth rate in alloy IN100. This is achieved by performing a heat treatment study to identify conditions leading to variation in the

size and volume fraction of γ'. These conditions are applied to compact tension (CT) specimens, which in turn have been examined under dwell loading cycles at 650°C and 700°C in air environment. The first section of the paper describes material and microstructure control followed by a description of intergranular crack growth experiments carried out on microstructures with different statistics of γ'. The effect of yield strength on intergranular crack growth rate is then examined numerically by utilizing a mechanistic based time-dependent crack growth model. This is then examined in terms of the γ' contributions to the total yield strength.

Material and Microstructure Control

The material employed in this study is Inconel 100 (IN100), a P/M processed nickel based superalloy having the composition (in wt%): Al 4.85, Ti 4.24, Co 18.23, Cr 12.13, Mo 3.22, V 0.71, Zr 0.071, B 0.02, C 0.072 [14]. The heat treatment of the as received material is a three stage process consisting of: i) solutioning at 1149°C for two hours then oil quenched, ii) stabilization at 982°C for one hour followed by fan cooling, and iii) aging at 732°C for eight hours then air cooling. The average grain size of the as received material is 5 μm (ASTM 12) and its microstructure, which is shown in Fig. 1a, includes γ'_p located at the triple points of the grain boundaries as well as within the grains and carbides mostly located along the grain boundaries. Micrographs revealing the precipitated phases were achieved with an etchant of 0.6g granulated Na_2O_2 and 50ml HCl applied for 7-10 minutes. The intragranular γ' particles, in Fig. 1a and 1b, exhibit a bimodal size distribution where the larger particles, γ'_s, appear cubical and the smaller ones, γ'_t, are spherical. The classification between secondary and tertiary γ' particles was determined using a threshold size of 50 nm. Sizes and volume fractions of the γ'_p are 1.7 μm and 20%, respectively, while statistics on the γ'_s and γ'_t are shown in Table 1. The precipitate sizes are reported as the average of the major and minor length of the particle.

A set of heat treatment experiments are conducted on the as received material in order to identify conditions that produce maximum and minimum volume fractions and sizes of the γ'_s and to investigate the long term stability of the microstructure, see details in reference [15]. These heat treatment conditions, listed in Table 1, are applied to CT specimens that will be tested to correlate their microstructure features and the corresponding intergranular cracking behavior. All heat treatments carried out in this study are sub-solvus conditions, thus the grain size, γ'_p size and volume fraction remained constant throughout the specimens. Microstructures corresponding to the selected heat treatment conditions are shown in Fig. 1. These micrographs are quantified through the use of image analysis software, results of which are presented in Table 1, in terms of volume fraction and size of γ'_s and γ'_t as a function of the heat treatment processes, respectively. General observations on the quantitative analysis of the heat treated microstructures, related to the volume fraction and particle size are detailed in references [15, 16].

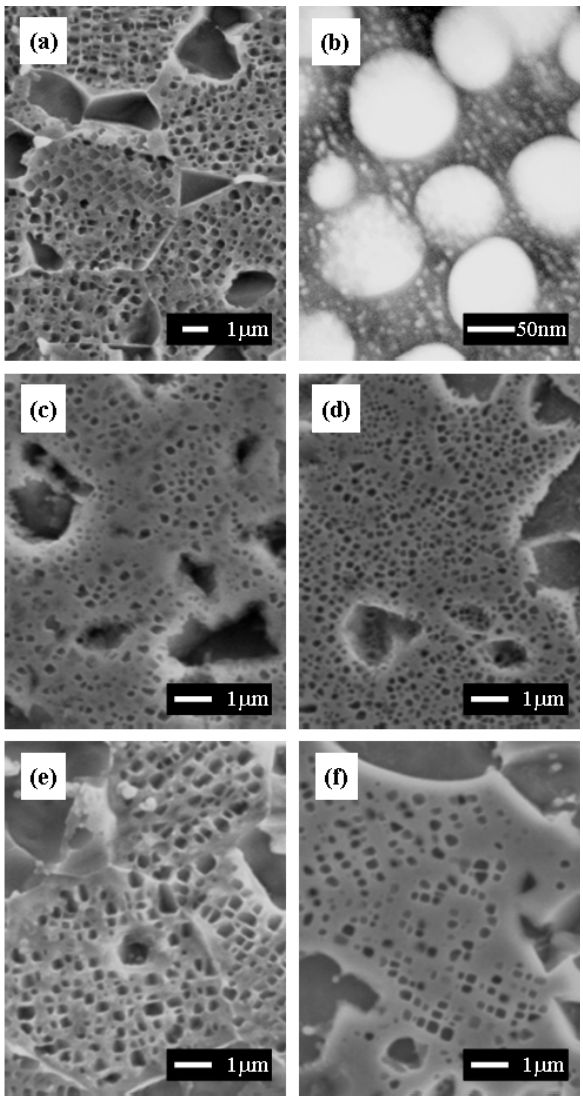

Figure 1: (a) Secondary electron image of the as received IN100 microstructure, etched with of 0.6g granulated Na_2O_2 and 50ml HCl applied for 7-10 minutes, showing γ'_s and γ'_t in the matrix, γ'_p and carbides located along the grain boundaries. (b) Transmission electron micrograph of the as received IN100 showing details of the γ'_t. Secondary electron images of etched IN100 microstructures showing size and volume fraction of different heat treated conditions; (c) overaged, (d) long term exposure, (e) very slow cooling from solutioning and (f) aging before stabilization, corresponding to those listed in Table 1.

Table 1: Yield strength (0.2% proof stress at 650°C, σ_y) and statistics (size, d and volume fraction, f) of secondary and tertiary γ' of the as received and heat treated IN100 microstructures.

	Specimen (Heat Treatment Sequence)	$f_{\gamma t}$ (%)	$d_{\gamma t}$ (nm)	$f_{\gamma s}$ (%)	$d_{\gamma s}$ (nm)	σ_y (MPa)
1	As received (1149°C 2hrs oil quenched, 982°C 1hr fan cooled, 732°C 8hrs air cooled)	11	23	29	208	1042
2	Overaged (815°C 75min cooled 1°C/min, 732°C 30hrs air cooled)	24	23	16	155	1095
3	Long term exposure (650°C 1500hrs air cooled)	21	29	19	130	1119
4	Very slow cooling from solutioning (1065°C 2hrs cooled 1°C/min for 10°C with 10min hold, repeating this cooling cycle to room temperature, 982°C 75min air cooled, 732°C 8hrs air cooled)	14	29	26	258	941
5	Aging before stabilization (1065°C 2hrs ice water quenched, 732°C 8hrs air cooled, 982°C 75min air cooled)	25	20	15	209	1035

Crack Growth Results

The role of microstructure on the crack growth process has been examined by carrying out two sets of dwell-fatigue crack growth experiments, as described in reference [16]. The first set is performed on CT specimens made of the as received material, while the second set was carried out on specimens that have been subjected to the heat treatment procedures described in Table 1. All tests were performed using servohydraulic material testing systems with the crack growth measurements being monitored using the potential drop technique. Pre-cracking was first performed at room temperature and testing was carried out at high temperature, in a resistance heating furnace. The loading cycle consists of 1 second loading, 1 second unloading and a dwell time of 0s, 100s and 7200s superimposed at the maximum load level. All tests were performed at a stress ratio of 0.1 at 650°C and 700°C in air environment. Results of the as received material are plotted as da/dN versus ΔK in Fig. 2, which shows that the crack growth rate is proportional to the dwell time.

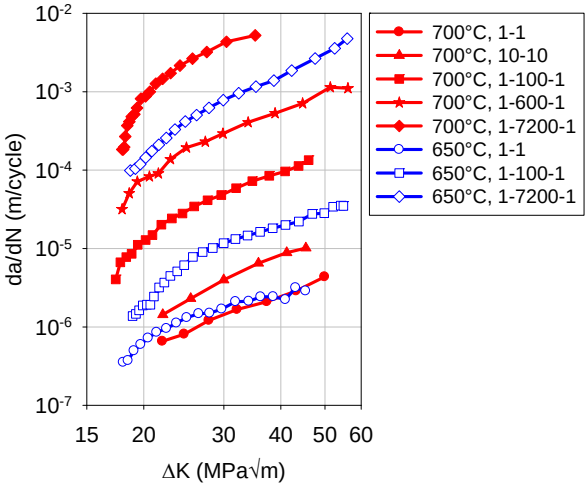

Figure 2: Crack growth rate as a function of temperature and hold time for as received material in terms of da/dN versus ΔK.

The transition between transgranular and intergranular fracture is defined by a transitional frequency, f_t, which is in the range of 0.06 to 0.12 Hz for the temperature range of 650°C to 700°C. For loading frequencies greater than f_t, the fracture mode is transgranular while for frequencies less then f_t, the fracture mode is intergranular. Focusing on the intergranular fracture region (i.e. frequencies less then transitional frequency), the da/dN versus ΔK can be plotted in terms of the corresponding crack growth speed, da/dt, versus maximum stress intensity, K_{max}, as shown in Fig. 3. This figure shows that for each of the two temperature levels, the crack growth curves with different hold time cycles are consolidated into a single curve. This indicates that for the same temperature, the intergranular growth increment per second is independent of the hold time duration. Thus, the thermally activated crack growth process is continuous and does not involve a damage incubation stage, suggesting that oxide formation is not a possible environmental damage mechanism.

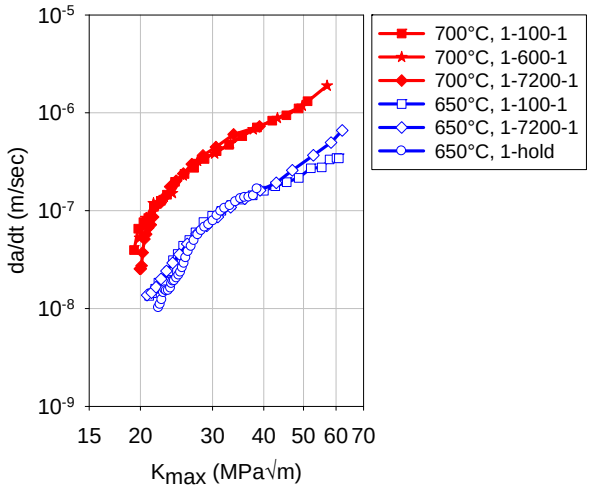

Figure 3: Crack growth rate as a function of temperature and hold time duration for as received material in terms of da/dt versus K_{max}.

The second set of the crack growth experiments is carried out on the four CT specimens with modified microstructures, see Table 1. These tests were performed in air environment at 650°C, with triangular loading frequencies of 0.5Hz and hold times at maximum load of 100s or 7200s. These frequencies are below the transgranular/intergranular transitional frequency and as such, the fracture path in each of the test specimens was intergranular and their da/dt versus K_{max} results are shown in Fig. 4. This figure shows that the crack growth rate of the modified microstructures at 650°C do not consolidate into a single curve.

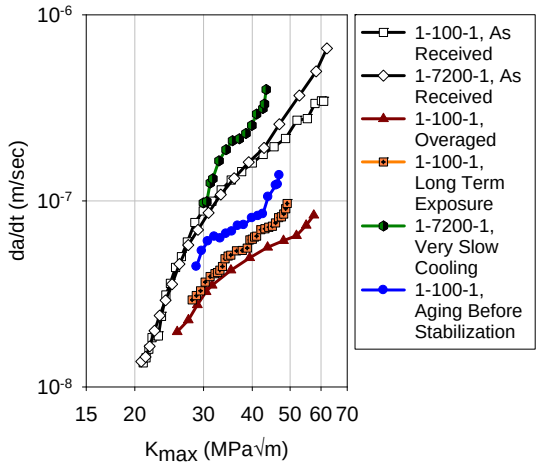

Figure 4: Crack growth rate in terms of da/dt versus K_{max} for different hold time tests conducted at 650°C on the as received and modified microstructures.

This suggests that variations of γ' statistics in the bulk material have altered the time-dependent deformation and damage mechanisms controlling the intergranular crack growth rate. This can be understood by the fact that high temperature intergranular cracking is generally described as the sum of two damage events related to environment and creep. The environmental damage component results from oxide formation and fracture or dynamic embrittlement due to oxygen diffusion. The work of Kirchhoff [15] on IN100 alloy precludes the oxidation route and shows that dynamic embrittlement is the active environmental damage mechanism in this alloy at 650°C. Furthermore, since the sub-solvus heat treatment procedures applied to the CT specimens listed in Table 1, did not result, as expected, in changes in grain size, GB morphology or GB phases, it could then be assumed that the GB activation energy in these modified microstructures has not been altered and therefore, the environmental damage contribution at the crack tip is the same for all the microstructures examined here at 650°C. Variations in the observed da/dt in Fig. 4 are thus considered to be mainly the outcome of creep related deformation and damage, involving GB sliding and/or cavitation. In this alloy, scanning electron microscopy observations carried out on the intergranular fracture surfaces show no evidence of cavities and, thus, sliding is considered to be the dominant mode of the GB deformation. Following the work of Ghonem and Maciejewski [17], the sliding rate, while dependent on the GB viscous characteristic, is also restricted by requirements of strain compatibility with the adjacent bulk material. In this bulk, the viscoplastic deformation is calculated from the knowledge of the viscous stress as a function of the back stress, isotropic hardening and yield strength [17]. Among these parameters, the yield strength is a measurable material parameter which is also directly influenced by γ' statistics. Considering that changes in the yield strength would influence the bulk deformation which in turn, alters the constraints imposed on the GB sliding rate, it is then possible to correlate the intergranular crack growth rate and the corresponding continuum yield. This conclusion could also be reached by examining the da/dt versus K_{max} relationship which, being a thermally activated process, can be written as:

$$\frac{da}{dt} = Ae^{-Q/RT} \tag{1}$$

where A is the frequency factor, Q is the apparent activation energy and is a function of K_{max}, R is the universal gas constant, and T is temperature in Kelvin. Considering T to be inversely proportional to the yield strength of the continuum, one could then correlate the crack growth and the yield strength, σ_y for different K_{max}, as shown in Fig. 5, for K_{max} ranging from 30 to 50 MPa√m, for the modified microstructures plus the as received material, tested at 650°C.

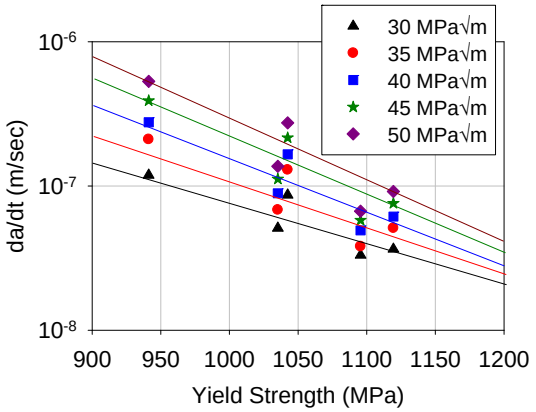

Figure 5: Crack growth rate, at five different K_{max} values, as a function of experimentally measured yield strength (0.2% proof stress) at 650°C for the as received and the heat treated conditions.

This figure shows that the continuum yield and the intergranular crack growth rate are inversely related. This type of relationship is similar to that discussed by Gayda and Miner [11] in their work on Astroloy at 650°C. As mentioned above, this relationship is assumed to be a result of a constraint imposed by the continuum viscous strain, as influenced by its yield strength, on the affected GB slip deformation. This concept will be examined in the analysis section of this paper. In this analysis, a numerical simulation of intergranular crack growth is performed to illustrate the nature of interactions between the continuum hardening and the intergranular crack tip sliding response and related crack growth rate. The role of precipitates on the crack growth becomes apparent from the knowledge that in the precipitate hardened IN100 alloy, the strength arises from solid solution strengthening in the γ matrix and precipitation hardening due to the ordered γ' precipitates which are coherently embedded in the matrix. The yield stress, σ_y, is, therefore, the sum of the combined contributions of the solid solution, σ_{ss}, and the strengthening components associated with tertiary and secondary γ' particles; $\sigma_{\gamma' t}$ and $\sigma_{\gamma' s}$, respectively. Hence, for the same K_{max}, da/dt is influenced by the sum, $(\sigma_{ss}+\sigma_{\gamma' t}+\sigma_{\gamma' s})$. This relationship can be used to determine the relative influence of γ'_t and γ'_s, through their corresponding yield component and will be discussed in the next section.

Analysis

The first part of this section deals with the numerical modelling of an intergranular crack path surrounded by a multi-scale viscoplastic continuum [16]. Results of this model will be used to illustrate the interactions between the continuum deformation, as governed by the corresponding yield and GB sliding. The second part of this analysis section will focus on identifying the individual contributions of γ'_s and γ'_t to the continuum yield strength [16].

Numerical Simulation: Effect of Yield Strength on GB Sliding and da/dt

This section explores the influence of the continuum yield and related viscoplastic strain on the deformation of the GB fracture path by performing a numerical simulation of intergranular crack growth using a cohesive zone model. In this, the GB fracture path is modeled as an interface, governed by viscoelastic traction-displacement laws, while the hardening behavior of the surrounding continuum is described by a multi-scale viscoplastic constitutive model. The GB interface is in direct contact with a near field continuum (represented by crystal plasticity formulations) surrounded by a far field zone (represented by non-linear kinematic hardening formulations); details of this model are given in references [16, 17]. The GB path, represented as an interface with a node to node contact, is described by traction-displacement laws in which the elastic displacement is the difference between the total (u_n, u_t) and inelastic displacements (u_c, u_s), in the normal and tangential directions; respectively. The inelastic displacement is equivalent to the GB sliding displacement, u_s, in the tangential direction and the opening displacement, u_c, in the normal direction is due to cavities. These traction-displacement laws are described as:

$$T_n = k_n \left(u_n - u_c \right) \tag{2}$$

$$T_t = k_t \left(u_t - u_s \right) \tag{3}$$

where the subscripts n and t represent normal and tangential directions, respectively, $T_{n,t}$ is traction and $k_{n,t}$ is cohesive stiffness. In the current analysis, $u_c = 0$, due to the absence of cavities. The GB sliding mechanism is described by a viscous flow law, in which the relative velocity of two sliding layers is written as [18]:

$$\dot{u}_s = \left(\delta / \eta \right) T_t \tag{4}$$

where δ is the GB thickness, η is the GB viscosity and T_t is the tangential stress. The GB viscosity can be derived as a function of the relaxation time, t_c, which is the time a dislocation can climb a distance λ [19] and η can then be written as:

$$\eta = \left(\delta E_{GB} / w_c \right) t_c = \left(\delta E_{GB} / w_c \right) \left(\lambda / v_c \right) \tag{5}$$

where E_{GB} is the unrelaxed shear modulus and w_c is the characteristic length over which GB sliding occurs, w_c is equal to 3 microns [17]. The climb velocity or dislocation velocity, v_c, is given by the Einstein mobility relation [20, 21, 22]:

$$v_c = M_d F = M_d T_t b \tag{6}$$

where M_d is the mobility of GB dislocations and F is the force per unit length acting on the dislocation and b is the Burger's vector. Substituting equations (5) and (6) into equation (4) yields the sliding rate in terms of dislocation mobility as:

$$\dot{u}_s = w_c \frac{M_d b}{E_{GB} \lambda} T_t^2 \tag{7}$$

Fracture occurs when the GB sliding displacement reaches a critical length, u_{crit}, which corresponds to a critical strain estimated as 4% [17].

The model simulation was performed on three cases of a P/M nickel based superalloy, tested at 650°C under sustained loading conditions. The yield strengths in these cases are selected as 0.75k, k and 1.25k, where k is the yield stress of the as received condition. These values were selected in order to encompass the range in variation in yield strength experimentally achieved; see Table 1 and Fig. 5. Details of the full parameter determination for the near and far field continuum and GB interface material models are given in [16, 17]. Results of the finite element model are grouped into node and element components. The node components, such as GB tractions and displacements, are outputs of the GB interface. The element components, stresses and extensions of elements located within the crystal plasticity zone of the continuum material, are outputs of the elements surrounding the crack tip. The element extension is taken as the average displacement of the nodes of the continuum element. Since damage in the normal direction is not considered in the IN100 alloy, only the components in the tangential direction are considered here. The tangential stress (S_{11}) and continuum element extension (U_1), in the element directly above the crack tip, as a function of time, are shown in Fig. 6a and 6b. These show that a material with higher yield strength, characterized by a larger stress and lower element extension at the crack tip, has less stress relaxation at the crack tip. This is assumed to provide higher constraints on the GB sliding. This is evident in simulation results pertaining to the GB traction and displacement. Fig. 7 shows the tangential displacement (u_t), traction (T_t) and GB sliding displacement (u_s) in the GB interface. The total tangential displacement, shown in Fig. 7a, is lower for a high strength material. As a result, the material with high yield strength and low tangential opening displacement has a lower tangential traction acting on the GB and lower sliding displacement, as shown in Fig. 7b and 7c; respectively. Furthermore, GB fracture is assumed to occur when the u_s reaches a critical displacement, u_{crit}. Thus, da/dt is proportional to GB sliding rate, described by the slope of the curve shown in Fig. 7c. A material with lower yield strength has a higher u_s, and larger GB sliding rate, reaching u_{crit} in a faster time, thus, has a faster crack growth rate.

The crack growth rate in each of the simulated conditions is calculated from Fig. 7c as the characteristic sliding length divided by the time to reach u_{crit}. Results of 5 simulated conditions are plotted in Fig. 8 in the form of normalized crack growth rate versus normalized yield. The trend in this figure is similar to that obtained experimentally in Fig. 5 indicating that the intergranular crack growth rate decreases with the increase in continuum yield strength.

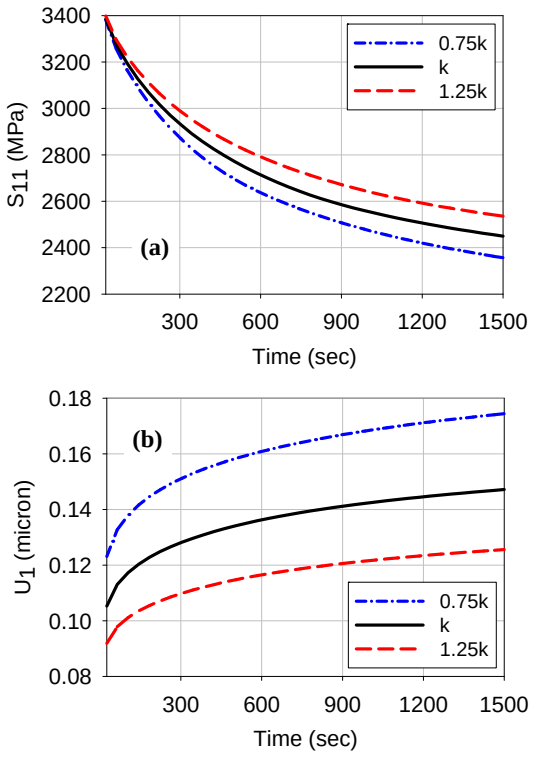

Figure 6: Tangential (a) stress and (b) element extension as a function of time in the element above the crack tip.

The next section will describe the influence of the precipitates' yield strength on da/dt by first calculating the yield strength due to tertiary and secondary precipitates; $\sigma_{\gamma' t}$ and $\sigma_{\gamma' s}$, respectively, and comparing their sum to the experimental yield. Once the validity of these theoretically calculated components are established, their individual contributions to da/dt will be examined.

Relative Influence of Precipitates' Yield Strength on da/dt

As mentioned in the previous section, the continuum yield is the sum of the contributions of the solid solution, σ_{ss}, and the strengthening components associated with tertiary and secondary γ' particles; $\sigma_{\gamma' t}$ and $\sigma_{\gamma' s}$, respectively. The work of Maciejewski et al [23] on the same alloy, IN100, has examined the solid solution hardening of the γ matrix, σ_{ss}, at 650°C on the basis of strengthening coefficients from elements in γ matrix. This work showed that σ_{ss} is approximately 298 MPa which is applicable to all the microstructures considered here. The contributions to the yield strength due to γ'_s and γ'_t occur as a result of dislocation/γ' particle interactions involving precipitate shearing and/or Orowan by-passing. These contributions are calculated as a function of the volume fraction, f and the particle size, d, for each of the precipitate populations. The first type of hardening occurs due to order strengthening, where the slip in the particle is accompanied by the formation of antiphase boundary and the increase in strength arises from the energy increase. Shearing of precipitates occurs when a particle is below a critical size, d_c, and the stress required for shearing, σ_{shear}, is less than that required for by-passing the particle. For the same volume fraction, the yield stress due to shearing is assumed to follow that for weakly coupled dislocations and is expressed as [24, 25]:

$$\sigma_{shear} = \theta MG\left(\frac{APB}{Gb}\right)^{3/2}\left(\frac{fd}{2b}\right)^{1/2} \tag{8}$$

where θ is a constant which equals 0.7, M is the Taylor factor equal to 3.06 [26], APB is the antiphase boundary energy, taken as 0.14 J/m^2 [27, 28], b is Burger's vector and G is the shear modulus. This equation is derived by considering a force balance across the leading and trailing dislocation. Once a coherent precipitate reaches a particle size greater than d_c, and taking into account the channel width, the stress required to loop the particle becomes less then that required to shear the particle, thus dislocation looping becomes the favorable interaction mechanism. The yield stress due to dislocation looping, σ_{loop}, is inversely proportional to the channel width, l, which can then be formulated as a function of d and f leading to the following expression [23, 24, 29]:

$$\sigma_{loop} = M\frac{Gb}{l} = MaGb\left(\frac{2f}{d(1-f)}\right) \tag{9}$$

where a is a material constant. The sum of the above two expressions for each of the precipitates, secondary and tertiary, assumes that precipitate shearing and looping mechanisms are operative on both tertiary and secondary particles depending on their average particle size with respect to the critical shearing/looping particle size, d_c. Transmission electron microscopy was utilized in the work of Maciejewski et al [23] to identify the nature of dislocation/particles interactions in heat treated specimens of IN100 alloy subjected to different strain rate and strain ranges. Results of this work showed that both the shearing and Orowan by-passing of γ' particles are active deformation mechanisms in IN100. The occurrence of either mechanism depends on the relative size of the particle with respect to a critical size, d_c, which is estimated to be 126 nm [23].

On the basis of these experimental observations, equations (8) and (9) are used to plot trends of yield stress for constant average volume fractions as a function of the average particle size for secondary and tertiary γ' precipitates represented by solid lines in Fig. 9a and 9b; respectively. In these two figures, the ascending part of each of the curves belongs to equation (8) which represents an increase in yield strength as d increases, while the descending part of the curve which belongs to equation (9) indicates a decrease in yield strength with an increase in the particle size. The intersection of these two curves, for a constant volume fraction, identifies the critical particle size, d_c. Fig. 9a shows that the average d_c corresponding to γ'_s is in the range of 100-126 nm for the volume fractions studied. Furthermore, Fig. 9b indicates that the γ'_t particles, for all microstructure conditions, fall within the shearing regime.

The stress components, $\sigma_{\gamma' t}$ and $\sigma_{\gamma' s}$, in Fig. 9, in addition to σ_{ss}, are plotted as a bar graph in Fig. 10 for each microstructure, showing the relative contributions of each of these components to the total yield strength. This figure shows that the average yield strength contribution due to γ'_s is 445 MPa while that due to γ'_t is 313 MPa. These stresses, $\sigma_{\gamma' t}$, $\sigma_{\gamma' s}$ and σ_{ss}, are summed to give the theoretically calculated yield stress. The validity of this sum is compared with that obtained experimentally showing a maximum error of 9.7%.

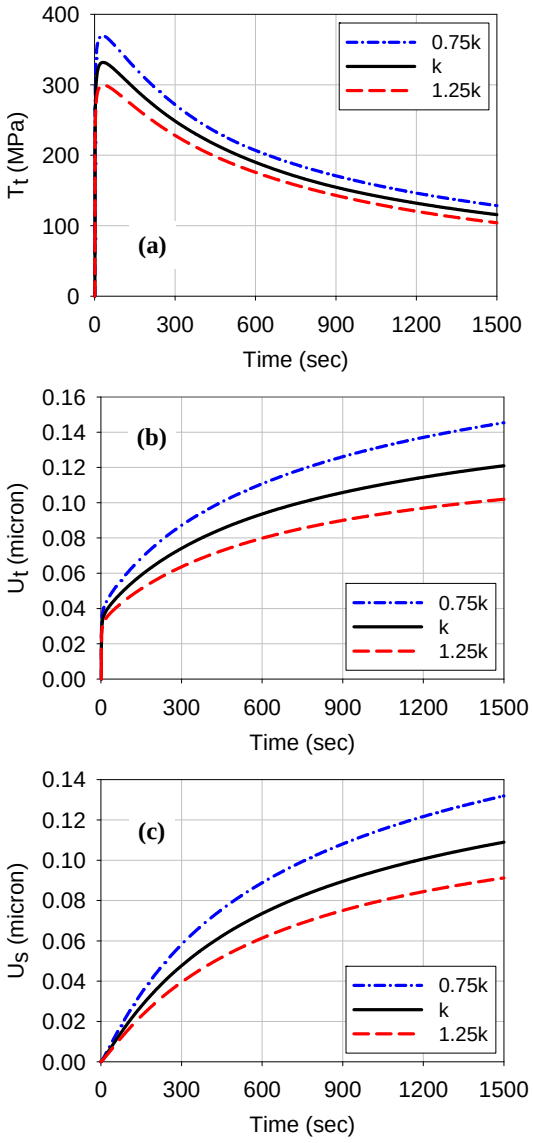

Figure 7: Tangential (a) displacement, (b) traction and (c) grain boundary sliding displacement as a function of time in the grain boundary at the crack tip.

These relative contributions of yield strength due to γ'_s and γ'_t on the intergranular crack growth rate are examined in Fig. 11a and 11b. The former figure shows that the trend of the theoretical sum of the yield stresses of the continuum versus the crack growth rate is similar to that of the experimental yield. The latter figure shows the relative correlation between the individual components, $\sigma_{\gamma' t}$ and $\sigma_{\gamma' s}$, and the da/dt. It is apparent from this correlation that the increase in each of the precipitates' yield strength provides a higher resistance to intergranular cracking. It is important, however, to observe that da/dt is more sensitive to variations in contribution from the tertiary precipitates as indicated by the slope of $\sigma_{\gamma' t}$ versus da/dt which is almost twice that of $\sigma_{\gamma' s}$ versus da/dt.

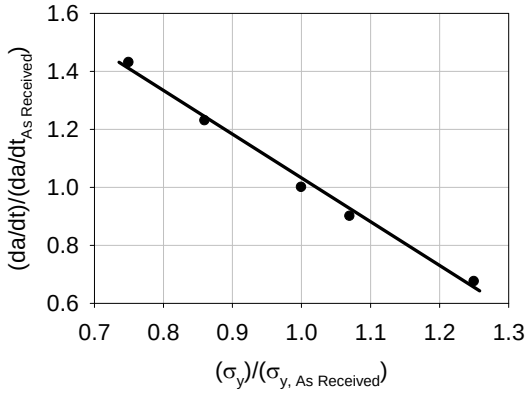

Figure 8: Crack growth rate, da/dt versus yield strength normalized to the as received microstructure, for the five simulated conditions.

Limitations of Yield Strength Enhancing Crack Growth Rate

Fig. 5 and Fig. 8 show that the intergranular crack growth rate decreases with the increase in yield strength. In order to explore the limitations of this trend, an additional heat treatment, aiming at generating a microstructure with very high yield strength is attempted. This heat treatment, termed quenched, consists of solutioning at 1135°C for 2hrs followed by water quenching, stabilization at 815°C for 2hrs followed by air cooling, and aging at 732°C for 8hrs followed by air cooling. This heat treatment sequence resulted in secondary and tertiary γ' particles with volume fractions of 27% and 13%, and sizes of 81 nm and 13 nm, respectively. The primary γ' has the same size and volume fraction as the as received microstructure. The yield strength of this heat treated microstructure is measured as 1252 MPa. A crack growth experiment was carried out on this microstructure at 650°C using a CT specimen of the same geometry as the ones used to generate Fig. 4. Results of this test when plotted with the five microstructures listed in Table 1, see Fig. 12, shows that a material with excessive yield strength has reversed the trend obtained in Fig. 11; i.e. an increase in the yield strength results in an increase in the crack growth rate. These two trends are illustrated in Fig. 13 for a K_{max} of 35 MPa$\sqrt{m}$.

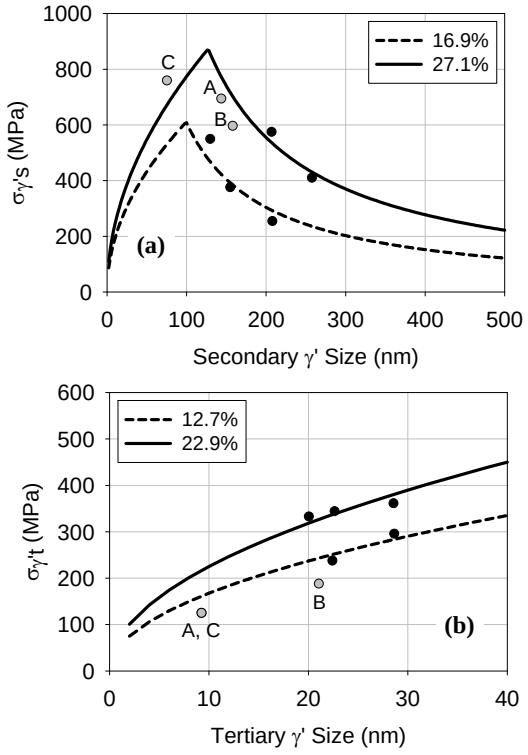

Figure 9: Yield stress of γ' particles, at 650°C, as a function of the average (a) secondary and (b) tertiary γ' particle size corresponding to the CT specimens (black circles) and three additional specimens (gray circles). In these three additional specimens, the primary, secondary, and tertiary γ' particles have volume fractions of 24%, 27%, and 8% respectively. For microstructures A, B and C, the secondary γ' sizes were (A: 144 nm, B: 159 nm, C: 76 nm) and the tertiary γ' sizes were (A: 10 nm, B: 21 nm, C: 10 nm).

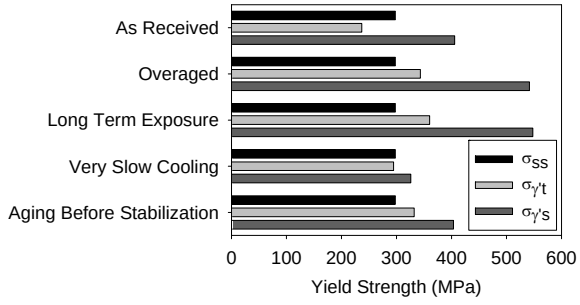

Figure 10: Bar graph of the total theoretically calculated yield stress components for the as received and heat treated IN100 microstructures at 650°C.

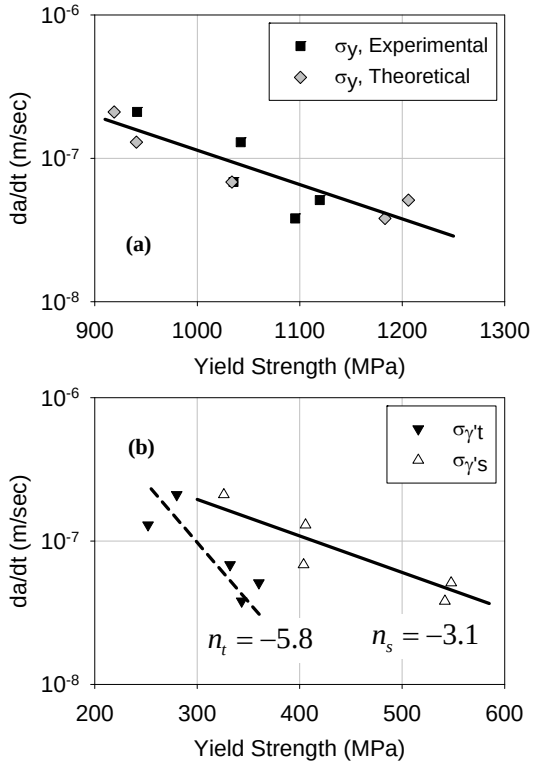

Figure 11: Crack growth rate, at a K_{max} of 35 MPa√m, versus the (a) total theoretical and experimental yield strengths, as well as, the (b) secondary and tertiary γ' yield strength components at 650°C.

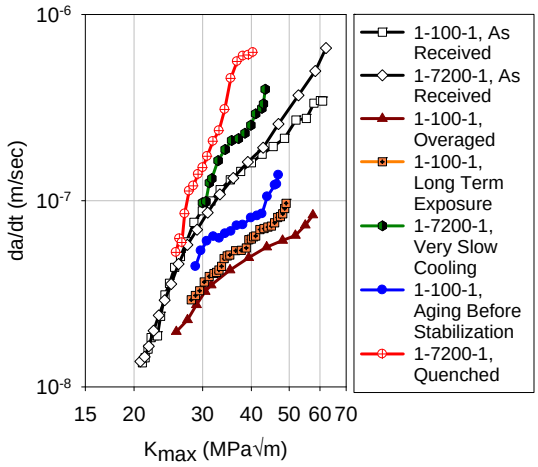

Figure 12: The crack growth rate of quenched microstructure with excessive yield strength compared with the crack growth rate of microstructures listed in Table 1. All tests are performed at 650°C.

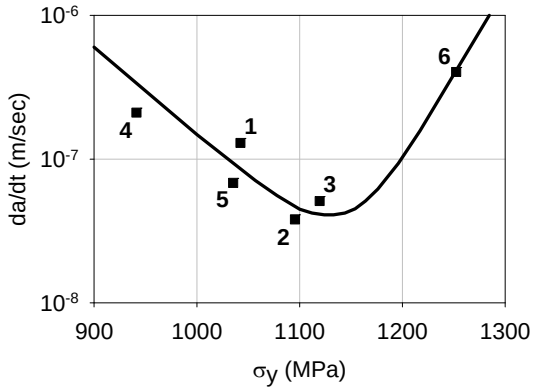

Figure 13: Crack growth rate, at a K_{max} of 35 MPa√m, as a function of experimentally measured yield strength (0.2% proof stress) at 650°C for the as received and heat treated conditions, corresponding to those listed in Table 1; (1) as received (2) overaged, (2) long term exposure, (4) very slow cooling from solutioning and (5) aging before stabilization. An additional heat treatment, 1135°C / 2hrs / water quenched, 815°C / 2hrs / air cooled, 732°C / 8hrs / air cooled, has been applied to a CT specimen labeled (6) in the graph.

The two opposite trends of the crack growth rate versus yield shown in the above figure indicate that da/dt decreases with the increase of σ_y, until reaching σ_y around 1150 MPa, after which the trend is reversed. The first part of this trend (σ_y < 1150 MPa), can be explained in relation to the positive effect of the hardening of a soft phase, where the highest da/dt and lowest σ_y is expected to correspond to the position of solid solution which has minor additional strengthening from γ' precipitates. Along this trend, as the yield strength increases, due to effects of secondary and tertiary precipitates, the grain boundary sliding, being the dominant deformation mechanism, becomes relatively restricted resulting in a slower GB sliding rate, thus a lower da/dt. Once the yield strength reaches a sufficiently large value, approximately 1150 MPa in this alloy studied here, the excessive pinning of the grain boundary results in apparent grain boundary embrittlement and a decrease in stress relaxation leading to higher crack growth rate. This second trend for σ_y > 1150 MPa, is in agreement with results of Telesman et al [10] which suggest that an increased stress relaxation at the crack tip corresponds to a lower crack growth rate.

Conclusions

A series of heat treatments were carried out on the IN100 alloy in order to identify conditions leading to variation in the size and volume fraction of γ' precipitates. These specific heat treatments are applied to CT specimens to regenerate the corresponding γ' statistics. Dwell-fatigue crack growth experiments are performed on these specimens at both 650°C and 700°C in air. Concerning the microstructure control, the various heat treatment cycles carried out in this study show that modifications in volume fraction and precipitate size can be achieved by variations in parameters including cooling rate from solutioning and stabilization stages, stabilization time, aging time and post aging thermal exposure, as well as, the order of the heat treatment cycles. These variations in the size and volume fraction of γ'_s are shown to influence the dwell crack growth rate. The main conclusions of this study are summarized as follows:

- Applying selected heat treatments result in variations in volume fractions, ranging from 15-29% and mean size, ranging from 130-258 nm in γ'_s, while corresponding variations in γ'_t range from 11-25% and 20-29 nm.
- For the as received microstructure, the intergranular crack growth rate at 650°C and 700°C, while temperature dependent, are independent of the hold time duration. This indicates that the cracking mechanism is a continuous process governed by combined dynamic embrittlement due to environment and creep damage associated with GB sliding.
- For the modified microstructures, the intergranular crack growth rate at 650°C is influenced by variations in the precipitate statistics.
- Focusing on the 650°C tests, a correlation is made between the crack growth rate, da/dt, and the continuum yield strength. This correlation is based on the assertion that changes in precipitates' statics affect the yield strength of the continuum which in turn, due to deformation compatibility requirements in the crack tip region, would influence the sliding rate of the GB fracture path.
- A mechanistic based intergranular crack growth model has been developed, simulating the growth rate of an interface surrounded by near and far field continuum zones, represented by crystal plasticity and non-linear kinematic hardening formulations, respectively. Results from this simulation suggest that a material with a higher yield strength, characterized by a larger stress and lower element extension or strain at the crack tip, has less stress relaxation at the crack tip, thus introduces a relatively high pinning effect on the GB motion. This suggests that a material with a high yield strength has less GB sliding displacement and consequently, a lower crack growth rate.
- The relative influence of precipitates' yield strength on da/dt has been established by calculating the contributions to the yield strength due to γ'_s and γ'_t by invoking yield strength formulae that consider dislocation/γ' particle interactions involving precipitate shearing and/or Orowan by-passing. The sum of these contributions, in addition to that of the solid solution, compared well with that obtained experimentally. The yield strength due to both precipitates is shown to be inversely proportional to da/dt. This relationship shows that the intergranular crack growth rate is more sensitive to the yield strength contribution from tertiary γ' compared with that of the secondary precipitates.

Acknowledgments

The authors acknowledge support provided by Dr. Agnieszka Wusatowska-Sarnek of Pratt & Whitney, East Hartford, Connecticut, during the heat treatment work in this study.

References

1. H. Ghonem, "Microstructure and Fatigue Crack Growth Mechanisms in High Temperature Titanium Alloys," *International Journal of Fatigue*, 32 (2010) 1448-1460.
2. H. Ghonem, T. Nicholas, and A. Pineau, "Elevated Temperature Fatigue Crack Growth in Alloy 718 – Part I: Effects of Mechanical Variables," *Fatigue and Fracture of Engineering Materials and Structures*, 5 (1993) 565-576.
3. H. Ghonem, T. Nicholas, and A. Pineau, "Elevated Temperature Fatigue Crack Growth in Alloy 718 – Part II: Effects

of Environmental and Material Variables," *Fatigue and Fracture of Engineering Materials and Structures*, 16 (1993) 577-590.
4. H.T. Pang and P.A.S. Reed, "Effects of Microstructure on Room Temperature Fatigue Crack Initiation and Short Crack Propagation in Udimet 720Li Ni-base Superalloy," *International Journal of Fatigue*, 30 (2008) 2009–2020.
5. J Telesman, P. Kantzos, J. Gayda, P.J. Bonacuse, and A. Prescenzi, "Microstructural Variables Controlling Time-Dependent Crack Growth in a P/M Superalloy," *Superalloys 2004*, ed. K.A. Green et al (Warrendale, PA: The Minerals, Metals and Materials Society, 2004), 215-224.
6. J.J. Schirra, P.L. Reynolds, E.E. Montero, E.S. Huron, K.R. Bain, and P.D. Mourer, "Effect of Microstructure (and Heat Treatment) on the 649°C Properties of Advanced PM Superalloy Disk Materials," *Superalloys 2004*, ed. K.A. Green et al (Warrendale, PA: The Minerals, Metals and Materials Society, 2004), 341-350.
7. H. F. Merrick and S. Floreen, "The Effects of Microstructure on Elevated Temperature Crack Growth in Nickel-based Alloys," *Metallurgical Transactions A*, 9 (1978) 231-236.
8. D. M. Knowles and D. W. Hunt, The influence of microstructure and environment on the crack growth behaviour of powder metallurgy Nickel superalloy RR1000, Met. and Mater. Trans.A, 33 (2002), 3165-3172.
9. L. Ma, K. M. Chang, and S. K. Mannan, "Effect of Prolonged Isothermal Exposure on Elevated-Temperature Time-dependent Fatigue Crack Propagation in INCONEL alloy 783," *Metallurgical and Materials Transactions A*, 35 (2002) 3465-3478.
10. J. Telesman, T.P. Gabb, A. Garg, P. Bonacuse, and J.Gayda, "Effect of Microstructure on Time Dependent Fatigue Crack Growth Behavior In a P/M Turbine Disk Alloy," *Superalloys 2008*, ed. R.C. Reed et al (Warrendale, PA: The Minerals, Metals and Materials Society, 2008), 807-816.
11. J. Gayda and R. V. Miner, "The Effect of Microstructure on 650°C Fatigue Crack Growth in P/M Astroloy," *Metallurgical Transactions A*, 14A (1983) 2301-2308.
12. M.P. Jackson, "Modelling and Characterisation of Phase Transformation in Nickel-base Superalloys," (PhD thesis, University of Cambridge, 1998).
13. W.W. Milligan, E.L. Orth, J.J. Schirra, and M.F. Savage, "Effects of Microstructure on the High Temperature Constitutive Behaviour of IN100," *Superalloys 2004*, ed. K.A. Green et al (Warrendale, PA: The Minerals, Metals and Materials Society, 2004), 331-340.
14. A. Wusatowska-Sarnek, M. Blackburn, and M. Aindow, "Techniquesfor microstructural characterization of powder-processed nickel-based superalloys. Material Science and Engineering A (2003), 360-390.
15. S. Kirchhoff, "Effects of Microstructure and Environment on Intergranular Crack Growth Behavior of a Powder Metallurgy Nickel Based Superalloy," (Master's thesis, University of Rhode Island, 2008).
16. K. Maciejewski and H. Ghonem, "The Relationship of Microstructure to Intergranular Crack Growth of a P/M Nickel-Based Superalloy at Elevated Temperatures," Int. J of Fatigue, 2012.
17. H. Ghonem and K. Maciejewski, "Mechanistic Modeling of Dwell Fatigue Crack Growth in P/M Nickel-Based Superalloys using a Cohesive Zone Approach," *Report, Metals Affordability Initiative Program*, AFRL, 2012.
18. F.W. Crossman and M.F. Ashby, "The Non-uniform Flow of Polycrystals by Grain Boundary Sliding Accommodated by Power-law Creep," *Acta Metallurgica*, 23 (1975) 425-440.
19. T. Kê, "Experimental Evidence of the Viscous Behavior of Grain Boundaries in Metals," *Physical Review*, 71 (8) (1947) 533-546.
20. F. Cosandey, "Grain Boundary Internal Friction and Relationship to Intergranular Fracture," *Journal De Physique*, C5 (10) (1988) 581-586.
21. E. Arzt, M.F. Ashby, and R.A. Verrall, "Interface Controlled Diffusional Creep," *Acta Metallurgica*, 31 (12) (1983) 1977-1989.
22. H.J. Frost and M.F. Ashby, *Deformation Mechanism Maps: the Plasticity and Creep of Metals and Ceramics* (Oxford, UK: Pergamon Press, 1982).
23. K. Maciejewski, and H. Ghonem, "The Effect of Microstructure on the Isotropic and Kinematic Hardening in a P/M Nickel-Based Superalloy at Elevated Temperatures," Material Science and Engineering A, 2012.
24. T. H. Courtney, *Mechanical Behavior of Materials*, (USA: McGraw-Hill Companies, Inc., 2000).
25. A.J., Ardell, "Precipitate Hardening," *Metallurgical Transactions A*, 16A (1985) 2131-2165.
26. J. A. Del Valle, R. Romero, and A.C. Picasso, "Bauschinger Effect in Age-hardened Inconel X-750 Alloy," *Materials Science and Engineering A*, 311 (2001) 100–107.
27. M. Heilmaier, U.Leetz, and B. Reppich, "Order Strengthening in the Cast Nickel-based Superalloy IN100 at Room Temperature," *Material Science and Engineering A*, (2001) 375-378.
28. M. Nemoto, W. H. Tian, and T. Sano, "Coherent Precipitation Strengthening by/in $L1_2$-ordered Phases," *Journal de Physique III*, 1 (1991) 1099-1117.
29. J.W. Martin, *Precipitation Hardening*, (Oxford: Butterworth Heinemann, 1998).